Journal of Peptide Science
J. Peptide Sci. **8**: 23–35 (2002)
DOI: 10.1002/psc.364

Conformational Flexibility of Three Cytoplasmic Segments of the Angiotensin II AT_{1A} Receptor: A Circular Dichroism and Fluorescence Spectroscopy Study

THELMA A. PERTINHEZ[a], REGINA KRYBUS[b], EDUARDO M. CILLI[c], ANTONIO C. M. PAIVA[c], CLÓVIS R. NAKAIE[c], LORELLA FRANZONI[d], GIORGIO SARTOR[d], ALBERTO SPISNI[a,d]* AND SHIRLEY SCHREIER[b]

[a] Center for Molecular and Structural Biology, LNLS, CP 6192, 13084-971, Campinas, Brazil
[b] Institute of Chemistry, Department of Biochemistry, University of São Paulo, CP 26077, 05599-970, São Paulo, Brazil
[c] Department of Biophysics, Federal University of São Paulo, Brazil
[d] Department of Experimental Medicine, Section of Chemistry and Structural Biochemistry, University of Parma, 43100 Parma, Italy

Received 23 July 2001
Accepted 5 October 2001

Abstract: The conformation of three synthetic peptides encompassing the proximal and distal half of the third intracellular loop (Ni3 and Ci3) and a portion of the cytoplasmic tail (*f*CT) of the angiotensin II AT_{1A} receptor has been studied using circular dischroism and fluorescence spectroscopies. The results show that the conformation of the peptides is modulated in various ways by the environmental conditions (pH, ionic strength and dielectric constant). Indeed, Ni3 and *f*CT fold into helical structures that possess distinct stability and polarity due to the diverse forces involved: mainly polar interactions in the first case and a combination of polar and hydrophobic interactions in the second. The presence of these various features also produce distinct intermolecular interactions. Ci3, instead, exists as an ensemble of partially folded states in equilibrium. Since the corresponding regions of the angiotensin II AT_{1A} receptor are known to play an important role in the receptor function, due to their ability to undergo conformational changes, these data provide some new clues about their different conformational plasticity.

Keywords: angiotensin II AT_{1A} receptor; circular dichroism; fluorescence; G-protein

INTRODUCTION

G-protein coupled receptors (GPCRs) form one of the largest and most important families of membrane-bound receptors [1]. It is widely accepted that, to untangle their structure–function relationship, an effective approach is to investigate segments of these large proteins [2–6].

The third intracellular loop (i3) and a portion of the *C*-terminal cytoplasmic tail of the

Abbreviations: AT_{1A}, type 1A angiotensin II receptor; Boc, *tert*-butyloxycarbonyl; Bzl, benzyl; CD, circular dichroism; DCM, dichloromethane; DIEA, N,N-diisopropylethylamine; DMF, N,N-dimethylformamide; *f*CT, segment of the AT_{1A} *C*-terminal cytoplasmic tail (residues 300–320); AcOH, acetic acid; GPRC, G-protein coupled receptor; HATU, N-[(dimethylamino)-1*H*-1,2,3-triazolo [4,5-b] pyridin-1-ylmethylene]-N-methylmethanaminium N-oxide; HOBt, 1-hydroxybenzotriazole; HPLC, high performance liquid chromatography; i3, third intracellular loop of AT_{1A}; MBHAR, 4-methylbenzhydrylamine resin; Ni3 and Ci3, *N*-terminal (residues 213–231) and *C*-terminal (residues 227–242) segments of i3, respectively; NMR, nuclear magnetic resonance; TBTU, 2-(1*H*-benzotriazol-1-yl)1,1,3,3-tetramethyluronium; TFA, trifuloroacetic acid; TFE, 2,2,2-trifluoroethanol; Z, benzyloxycarbonyl.

*Correspondence to: A. Spisni, Department of Experimental Medicine, University of Parma, Via Volturno, 39, Parma, Italy; e-mail: aspin@unipr.it

Contract/grant sponsor: FAPESP.
Contract/grant sponsor: CNP_q.
Contract/grant sponsor: MURST.
Contract/grant sponsor: CNR; Contract/grant numbers: 98.00517.CT04; 99.02668.CT04.

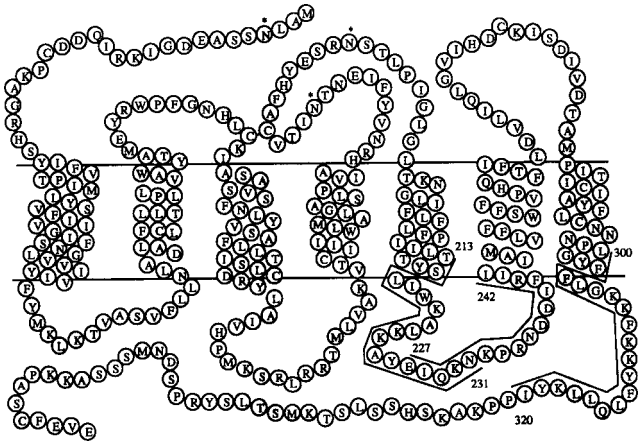

Figure 1 Amino acid sequence and schematic representation of the rat AT_{1A} receptor. The synthetic peptides studied in this work, named Ni3 (residues 213–231), Ci3 (residues 227–242) and *f*CT (residues 300–320), are indicated by solid lines.

angiotensin II AT_{1A} receptor (AT_{1A}) are known to be involved in receptor activation and G-protein selection and coupling [7–11]. Based on this evidence, we concentrated on three segments of those cytoplasmic domains (Figure 1) that site-specific mutagenesis and chimera expression [10–13] indicate are essential for the receptor's function: (i) the proximal part of the i3 loop (residues 213–231, TSYTLIWKALKKAYEIQKN-NH_2, Ni3), (ii) a segment of the *C*-terminal tail (residues 300–320, LFYGFLGKKFKKYFLQLLKYI-NH_2, *f*CT) and (iii) the distal part of the i3 loop (residues 227–242, EIQKNKPRNDDIFRII-NH_2, Ci3). Segments (i) and (ii), as free peptides, are able to compete with the receptor for G-protein activation [7, 8] while segment (iii), although inactive when tested as a free peptide, turns out to be an essential part of the i3 loop for AT_{1A} activation and coupling [7].

Previous studies carried out by ^{1}H-NMR [14, 15] showed that the synthetic receptor's segments, in water at acidic pH, exist in a random coil conformation and that, in 30% TFE, while *f*CT and Ni3 are able to fold into an α-helical structure, Ci3 exhibits an ill-defined conformational behaviour.

Recognizing that the expression of some biological function implies the existence of stable or inducible structural determinants, we have been prompted to investigate, by CD and fluorescence spectroscopies, whether physiological parameters such as pH, ionic strength and dielectric constant, can elicit *in vitro* secondary and tertiary structures representative of the molecular events that *in vivo* are expected to be associated with the function of the receptor complex machinery.

MATERIALS AND METHODS

Peptide Synthesis

The peptides TSYTLIWKALKKAYEIQKN (Ni3), EIQKNKPRNDDIFRII (Ci3) and LFYGFLGKKFKKYFLQLLKYI (*f*CT) (Figure 1) were synthesized manually accordingly to the standard Boc/Bzl strategy [16, 17] *p*-Methylbenzhydrylamine-resin (0.79 mmol/g) in a 0.4 mmol scale was used as the solid support and the side-chain protecting groups employed were: Bzl (S and T), 2-Br-Z (Y), cyclohexyl (D and E), 2-Cl-Z (K), *p*-toluenesulphonyl (R) and formyl (W). Briefly, the α-amino group deprotection and neutralization steps were performed in 30% (v/v) TFA/DCM for 30 min and in 10% (v/v) DIEA/DCM for 10 min. The coupling step was carried out using a three-fold excess of the acylating reagents TBTU/DIEA [18] and HATU/HOBt [19] when recoupling was necessary. On the basis of a previous report [20] correlating the solvation of resin beads with several factors such as the peptide content, the peptide sequence and the polarity of the medium, during the coupling in the resins containing up to about 30% peptide (weight/weight) or higher, we used as solvent systems, 50% v/v DCM/DMF and 30% DMSO/NMP, respectively. Cleavage of the peptide from the resin was carried out in HF : *o*-cresol : dimethylsulphide (9 : 0.5 : 0.5) at 0 °C for 90 min. In the case of the Trp-containing Ni3 sequence, ethanedithiol was added to the HF mixture in 5% (v/v) final solution. The resins were rinsed with ethyl acetate and peptides were extracted with 5% AcOH and lyophilized. Purification of the peptides was carried out on a Waters 510 HPLC instrument using a Vydac C_{18} semi-preparative column

(25 × 250 mm, 300 Å pore size, 15–20 μm particle size). The peptides were dissolved in 5% AcOH, sonicated and centrifuged at 10 000 × **g**. After filtration, the solution was loaded onto the column and eluted with solvent A, H_2O containing 0.1% TFA and solvent B, H_2O containing 60% acetonitrile and 0.08% TFA. The flow rate was 10 ml/min and absorption was detected at 210 nm. Linear gradients ranging from 45% to 85% of B, for Ni3 and *f*CT, and 25%–65% of B, for Ci3, were applied over a period of 2 h.

Analytical HPLC

A Vydac C_{18} column (4.6 × 150 mm, 300 Å pore size, 5 μm particle size) was used with solvent A, H_2O containing 0.1% TFA and solvent B, H_2O containing 60% acetonitrile and 0.08% TFA. Flow rate was 1.5 ml/min and the absorption was detected at 220 nm. A linear gradient ranging from 5% to 95% of B was applied over a 30 min interval. In these conditions, the peptides Ni3, Ci3 and *f*CT eluted in 19, 17 and 25 min, respectively.

Amino Acid Analysis

The peptides Ci3 and *f*CT were hydrolysed with 6 N HCl and the Trp-containing Ni3 with 3 N *p*-toluenesulphonic acid (both procedures at 110 °C for 72 h) followed by neutralization with 2 N NaOH, in a Pyrex tube with plastic Teflon-coated screw cap. The hydrolysed products were analysed in a Beckman 6300 Amino Acid Analyzer. The analyses showed the expected amino acid composition for each of the peptides.

Mass Spectrometry

Peptides were analysed by Matrix Assisted Laser Desorption Ionization (MALDI) on a Micromass Spectrometer, model TofSpec SE, using α-cyano-4-hydroxycinnamic acid as matrix. The molecular weights found for peptides Ni3, Ci3 and *f*CT were, m/z: 2297.9 Da ($M^+ + 1$) (theoretical value: 2297.7), 1998.4 Da ($M^+ + 1$) (theoretical value: 1998.3) and 2657.8 Da ($M^+ + 1$) (theoretical value: 2657.3), respectively.

Circular Dichroism Spectroscopy

Far-UV CD spectra were recorded on a Jasco J-715 equipped with a Peltier system PTC-348 WVI for cell temperature control and on a Jobin Yvon CD6 spectropolarimeter. Ellipticity is reported as the mean residue molar ellipticity, [θ] (deg cm^2 $dmol^{-1}$). Peptide concentration was determined either based on the peptide content derived from the amino acid analyses or spectrophotometrically using the extinction coefficients of the Tyr and/or Trp residues at 276 nm, $\varepsilon_{Tyr} = 1390$ M^{-1} cm^{-1} and $\varepsilon_{Trp} = 5455$ M^{-1} cm^{-1}, respectively [21]. The percentage of α-helix was estimated using the mean residue molar ellipticity at 222 nm ($[\theta]_{222}$) [22].

Fluorescence Spectroscopy

Fluorescence spectra were recorded using a Hitachi 1050 spectrofluorimeter at 25 °C. In the case of *f*CT the excitation wavelength was set at 274 nm and, to avoid the interference of the water Raman peak at 302 nm, the intensity of the Tyr fluorescence was measured at 310 nm. In the case of tyrosinate, the fluorescence intensity was measured at 370 nm to eliminate any artefact due to residual Tyr fluorescence. For Ni3, Trp was excited at 295 nm. Emission and excitation slits were set at 5 nm band-pass; cells were 1 cm pathlength. Corrections were made for inner filter effects [23]. Fluorescence quenching data were analysed using the Stern-Volmer approach for pure collisional or pure static quenching. In the case of mixed type quenching the data were fitted according to Eftink and Ghiron [24].

Analysis of the pH Titration

The data of the pH titration for both the CD and fluorescence experiments were fitted by a non-least square regression analysis using the Henderson–Hasselbach equation with two pK_a values.

RESULTS AND DISCUSSION

The C-Terminal Tail (*The fCT Segment*)

Figure 2A shows that at pH 4.0 *f*CT exists in an extended form and folds into an α-helical conformation upon increasing the pH. The conformational transition begins at about pH 6.5 and the negative ellipticity increases steadily up to pH 7.7 (Figure 2A, inset). At pH 8.0 a sudden increase of the spectral intensity occurs. Subsequently, at pH 8.8, there is an abrupt decrease of the ellipticity associated with a significant change of the CD profile (Figure 2B) suggesting the onset of self-association. Overall, the data confirm the expected pH dependence of the peptide conformation due to the

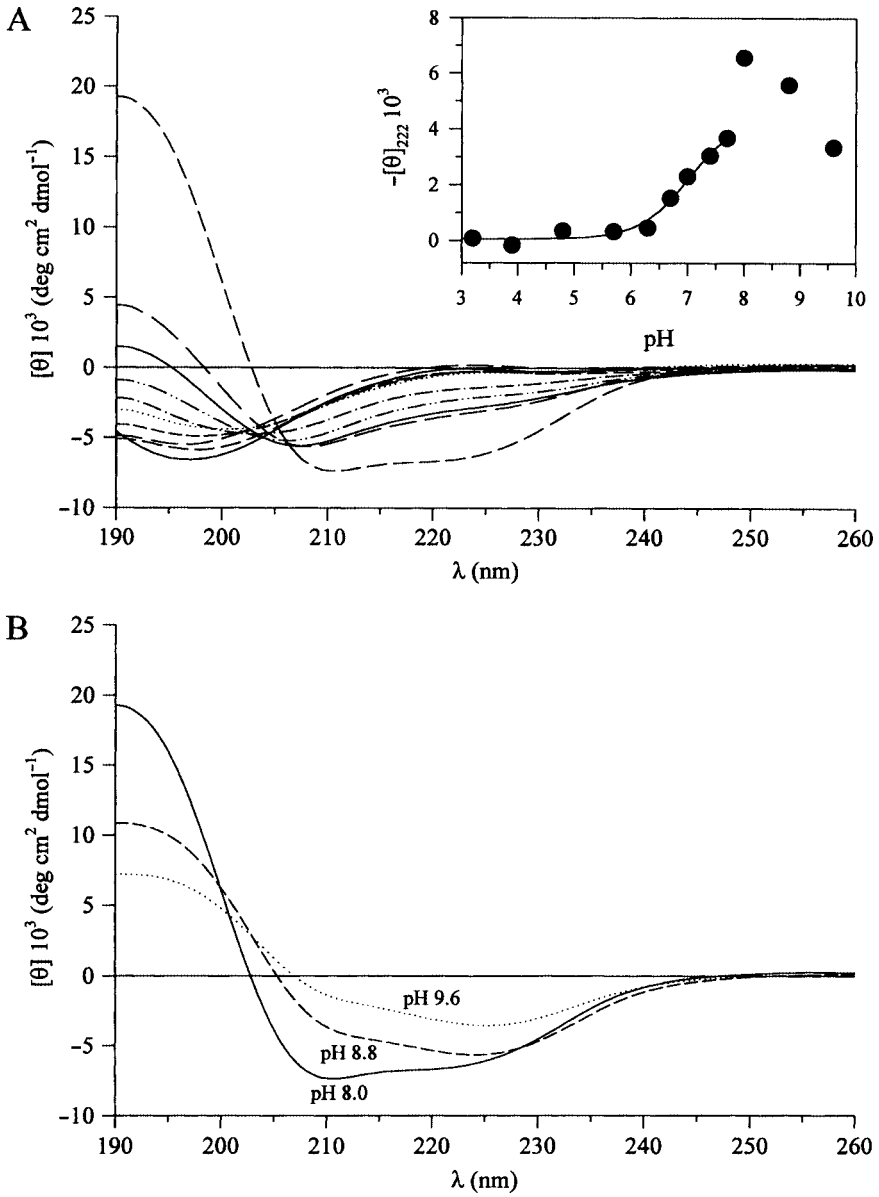

Figure 2 CD spectra of 0.12 mM *f*CT in water as a function of pH at 20 °C. A: pH range 3.0–8.0 (acid to basic pH from top to bottom at 222 nm). Inset: $-[\theta]_{222}$ as a function of pH; B: pH values of 8.0 (———), 8.8 (- - - -) and 9.6 (·····).

presence of several ionizable side chains. They also indicate that hydrophobic interactions between the Tyr and Leu residues at positions $(i, i+3)$ or $(i, i+4)$, (Tyr3-Leu6, Tyr13-Leu17, Ley17-Tyr20), combined with electrostatic interactions, most likely between the Lys and Tyr residues, might be involved in helix stability and may also favour coiled-coil formation [25–29]. In addition, the intra- and intermolecular salt bridges, besides being important for helix stabilization [30], contribute to neutralize the peptide surface, further justifying its enhanced aggregation capacity.

To corroborate this hypothesis we examined the pH dependence of the peptide fluorescence (Figure 3). The phenol side chain of the Tyr residues is in equilibrium with its dissociated form, with a $pK_a \approx 10$ which drops to $pK_a \approx 4.5$ in the excited state [31]. Since the fluorescence emission maximum of the former lies between 303–305 nm while the tyrosinate form emits in the range 340–350 nm [32], we have been able to monitor the pH behaviour of the two species. As indicated in the Materials and Methods section, to avoid spectral interference, the fluorescence intensity was

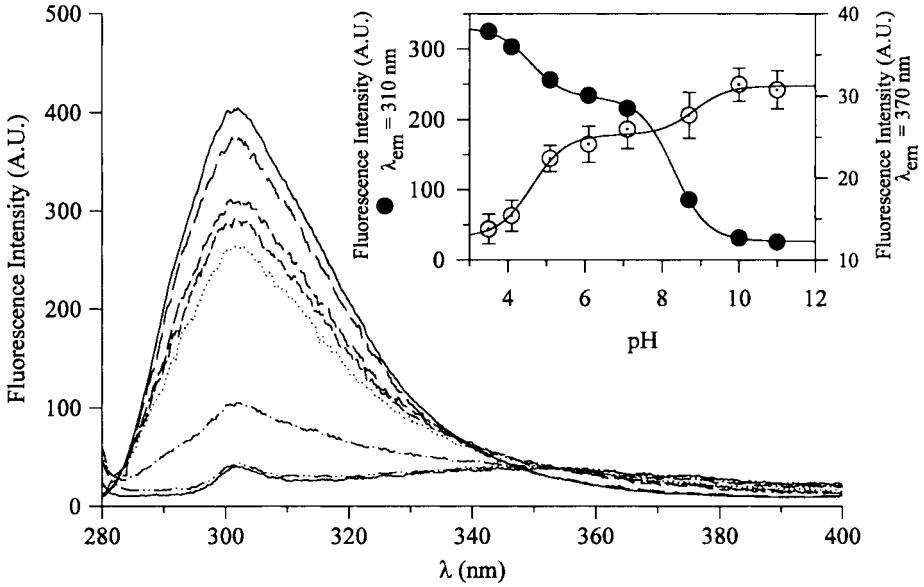

Figure 3 Fluorescence spectra of *f*CT (1.18×10^{-5}M) in water as a function of pH, (acid to basic pH from top to bottom); excitation: 274 nm. Inset: Plot of the fluorescence intensity as a function of pH at the emission wavelengths 310 nm (●) and 370 nm (○).

measured at 310 nm and at 370 nm for Tyr and tyrosinate, respectively. The first decrease in the fluorescence intensity, measured at 310 nm, at about pH 4.6 ± 0.1, coupled with a fluorescence increase measured at 370 nm (Figure 3, inset), is indicative of the ionization of the Tyr hydroxyl group in the excited state. As for the second decrease of the fluorescence intensity at 310 nm at about pH 8.5 ± 0.3, and the concomitant increase detected at 370 nm, is can be associated with ionization in the ground state. The pK_a decrease, observed in the ground state, is suggestive of the onset of inter- and/or intramolecular interactions. These results are consistent with the CD data and support the hypothesis that hydrophobic and electrostatic side chain interactions are responsible for the peptide tendency to form intermolecular aggregates.

The Stern-Volmer plots of the Tyr fluorescence quenching, carried out at pH 4.0, 7.4 and 8.5, using acrylamide, indicate that the quenching mechanism is purely collisional (data not shown). The quenching constants (Table 1), show that acrylamide efficiency decreases from pH 4.0 to pH 8.5, and that, already at neutral pH, the quencher accessibility to the Tyr residues is reduced indicating that partial aggregation is already present.

To further ascertain the role of electrostatic and hydrophobic interactions in the regulation of the peptide folding pathway, the dependence of the secondary structure on ionic strength was studied at pH 4.0 and 7.4 (Figure 4). At pH 4.0, the data evidence the existence of a two-step transition (Figure 4, inset). Up to 1.5 mM NaCl there is a smooth transition from the extended to a stable intermediate state. This behaviour, combined with the absence of an isodichroic point, suggests the presence of various conformations in equilibrium. A second, steeper transition takes place between 2.5 and 4.0 mM NaCl, indicating a further enhancement of the peptide ordered secondary structure.

Interestingly, when the titration is carried out at pH 7.4, only a smooth transition is observed

Table 1 Stern-Volmer Quenching Constants, K_{sv}, for the Tyr Residues in *f*CT and the Trp Residue in Ni3 Obtained using Acrylamide as Quencher

pH	$K_{sv}(M^{-1})$	
	*f*CT	Ni3
4.0	14.4	15.3
7.4	10.6	8.1
		3.0[a]
8.5	9.3	—
9.3	—	7.5

[a] At pH 7.4 the Stern-Volmer plot for Ni3 is not linear. Therefore the data have been analysed according to [24].

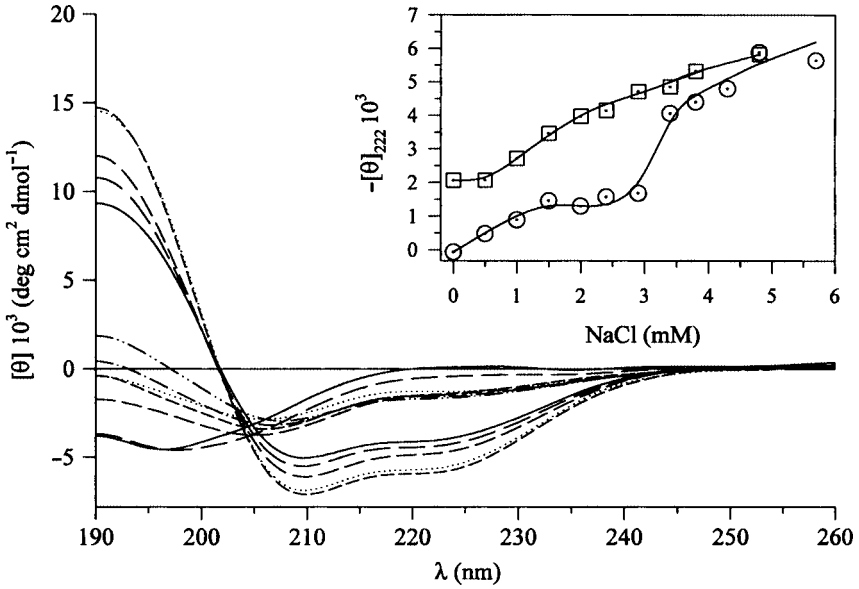

Figure 4 CD spectra of 0.12 mM *f*CT in water at pH 4.0 and 20 °C as a function of NaCl concentration (NaCl concentration increasing from top to bottom at 222 nm). Inset: $-[\theta]_{222}$ as a function of NaCl concentration at pH 4.0 (○) and pH 7.4 (□).

starting at 1 mM NaCl, which is followed by a steady increase of the ellipticity up to 4.5 mM NaCl, where it reaches a value similar to the one obtained when carrying out the salt titration at pH 4.0. The loss of biphasic behaviour (Figure 4, inset) suggests that the intermediate state observed at pH 4.0 depends on electrostatic interactions.

Overall, the results show that at physiological pH *f*CT exists as an ensemble of conformations characterized by partial helical folding and capable of acquiring supramolecular organization.

The i3 Loop

The Ni3 segment. In water, at pH 3.8, Ni3 displays a CD spectrum typical of a peptide in a predominantly random conformation (Figure 5A). Different from *f*CT, the variation of the peptide concentration in the range 0.15–1.5 mM does not cause any aggregation (data not shown).

Nonetheless, because of its charged residues and similarity to *f*CT, Ni3 is expected to be sensitive to pH and ionic strength. In fact, on increasing the pH, we observed a fold of Ni3 into a helical conformation up to a maximum helical content of ca. 66% (Figure 5A). An initial minor conformational transition at pH 6.7 ± 0.1 can be related to the dissociation of Glu15. The increase of its apparent pK_a may reflect the formation of salt bridges with the protonated Lys residues in positions $(i+3)$ and $(i-3)$. The second transition, at pH 9.5 ± 0.1, suggests that the dissociation of the four Lys residues and the consequent reduction of the helix destabilizing electrostatic repulsions [25] plays a crucial role in the folding process. Interestingly, the pH at which this conformational transition takes place is significantly higher than for *f*CT.

The behaviour of the Trp7 fluorescence as a function of pH is reported in Figure 5B. The first weak decrease of the fluorescence intensity at pH 6.0 ± 0.4 is likely to reflect an initial interaction with Tyr3 as a result of the conformational change induced by the ionization of Glu15. The second main decrease, centred at pH 9.4 ± 0.1, might be due to a stronger interaction, favoured by the peptide folding, with the nearby Tyr3 and Lys8. However, considering that the absence of a blue shift in the fluorescence emission spectrum indicates that, while the peptide folds, the Trp residue remains in a polar environment, another factor justifying the fluorescence decrease could be the movement of the Trp side chain closer to the peptide bonds.

The Stern-Volmer constants for the acrylamide quenching experiments, carried out at various pHs, are reported in Table 1. The quenching mechanism at pH 4.0 and 9.3 is of the collisional type. At pH 7.4, the non-linearity of the plot (data not shown) indicates the presence of an additional static component. The analysis of the data [24] yielded a K_{SV} of 8.1 M^{-1} and 3.0 M^{-1} for the collisional and static components, respectively. This result is

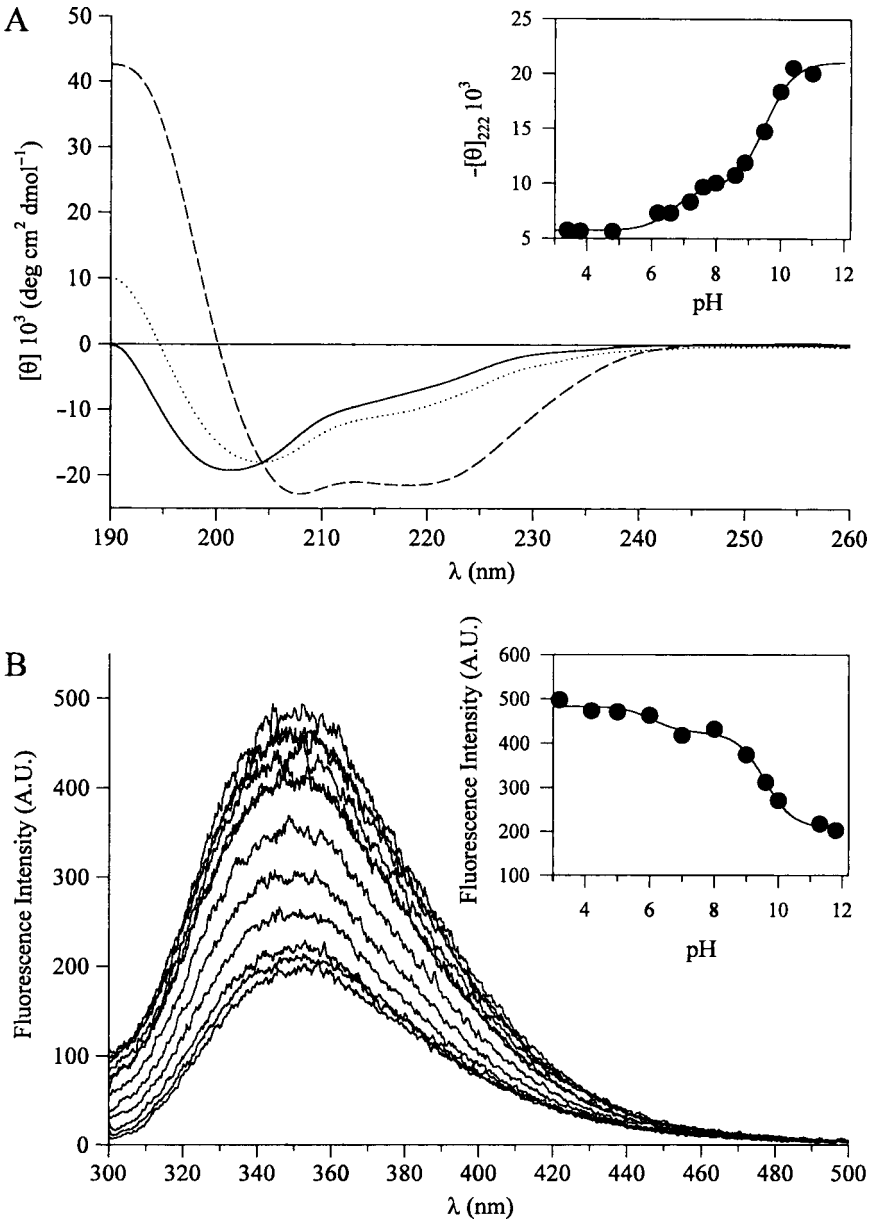

Figure 5 A. CD spectra of 0.15 mM Ni3 in water as a function of pH, at 20 °C; pH values of 3.8 (———), 7.2 (·····) and 10.4 (- - - -). Inset: $-[\theta]_{222}$ as a function of pH; B. Fluorescence spectra of Ni3 (2.2×10^{-5} M) in water (acid to basic pH from top to bottom), λ_{exc} 295 nm. Inset: fluorescence intensity at 350 nm as a function of pH.

therefore suggestive of a heterogeneous population of Trp residues. Since each Ni3 peptide molecule carries only one Trp residue, these data also indicate the coexistence of various conformational states in agreement with the absence of an isodichroic point in the CD spectra. In addition, because the CD data do not indicate any aggregation process, the decreased accessibility at basic pH can be considered a confirmation of the proposed onset of intramolecular interactions.

As for the dependence of the peptide conformation on ionic strength, although Ni3 is positively charged, the alterations of the CD spectra, both at pH 4.0 and 7.4, are not significant (data not shown). It is possible that conformational changes might occur at a higher salt concentration. However, for the purpose of the present work, it is noteworthy that, in the same ionic strength range, Ni3 and *f*CT, though they both contain a patch of Lys residues (Figure 6), behave in a distinct manner.

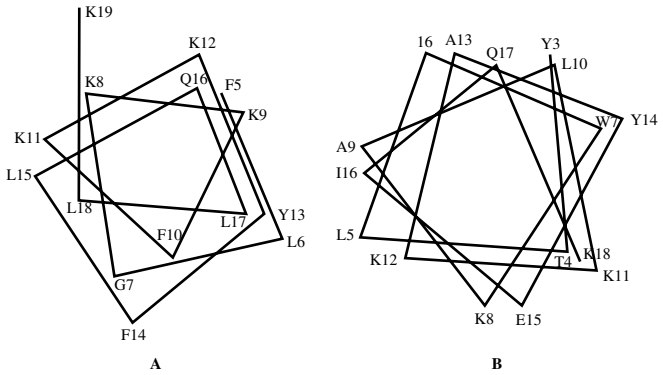

Figure 6 Helical wheels based on the structure determined by NMR in 70% H_2O: 30% TFE. A. *f*CT at 5 °C (14); B. Ni3 at 25 °C (15).

Indeed, the NMR-based helical wheel, obtained in 30% TFE [15] (Figure 6B), evidences that in the patch of Lys residues there are also Glu and Thr residues that, because of their significative electron density, at the low salt concentrations tested could account for the reduced ion–peptide interaction.

To better define the intrinsic propensity of the peptide to fold into a helical structure, we tested the effect of TFE as a co-solvent [33, 34]. The TFE/H_2O titration at pH 4.0 (Figure 7A) shows that the coil to helix transition has already started at 10% TFE. The extent of the helical conformation increases up to 30% TFE, reaching a value of about 59%. In the TFE range 20%–100% the CD spectra show an isodichroic point at 201.2 nm, confirming the existence of a two-state transition. Moreover, the sigmoidal shape of the plot of $[\theta]_{222}$ vs % TFE (Figure 7A, inset) is suggestive of a strong cooperativity of the folding. The CD profile of the peptide was investigated at various temperatures in 30% TFE to evaluate the helix stability. This experimental condition was chosen because, while at this TFE concentration the peptide appears to have already reached a stable folded conformation, yet enough water molecules are present to guarantee an efficient interaction with the peptide backbone. Figure 7B shows a linear increase of the ellipticity with decreasing temperature. However, the relatively small variation of the helical content (from 35% to 59%), suggests a very stable helical structure. Moreover, since the decrease in ellipticity is associated with an insignificant shift of the two π-π^* transitions (192 nm and 208 nm), we can hypothesize that, upon increasing the temperature, rather than an unfolding process, what is occurring is only a loosening of the helical structure that causes a weakening of the helical macrodipole.

In summary, Ni3 turns out to be a peptide characterized by a certain degree of conformational flexibility in water. However, if its conformational space is restricted, as happens in TFE, it acquires a quite stable helical structure able only to fluctuate between a loose and a tight state.

Comparison of fCT and Ni3 Helicity

Although *f*CT and Ni3 share some common features such as the presence of Lys patches and the ability to form amphipathic helices, they show a distinct behaviour with respect to their response to ionic strength and their ability to elicit intermolecular interactions.

The helical content for Ni3 and *f*CT in H_2O at pH 8.0 is 38% and 28%, respectively. However, in 30% TFE at 5 °C the two peptides have the same helicity (ca. 60% helical content).

This apparent inconsistency can be explained if the CD data are analysed using, as a measure of the α-helix content, the ratio R_2 between the ellipticity at 222 nm and that of the negative maximum in the range 195–210 nm [35] Knowing that R_2 tends to 1 for 100% helix and decreases for a lesser helical content we find, in contrast to the previous estimate based on $[\theta]_{222}$ that, at pH 8.0, *f*CT presents a higher content of helical structure than Ni3, $R_2 = 0.88$ and 0.52, respectively. Moreover, the measurable limiting values of R_2 (Figure 8) suggest that, in water, the two peptides possess comparable helicity.

These results can be rationalized considering that when the *f*CT molecules begin to fold, due

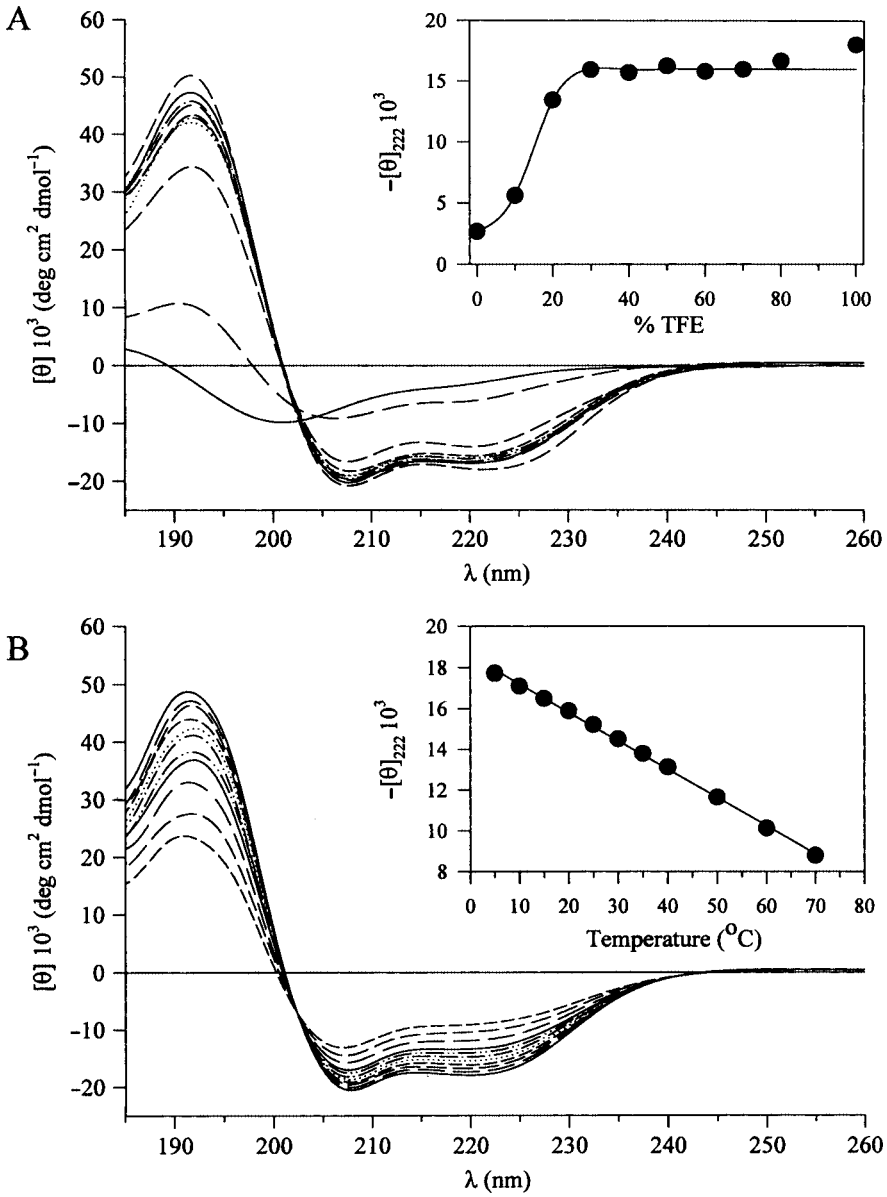

Figure 7 A. CD spectra of 0.15 mM Ni3 in water at pH 4.0 and upon addition of TFE in the concentration range 0–100% (v/v) at 20 °C (TFE concentration increasing from top to bottom at 222 nm). Inset: $-[\theta]_{222}$ as a function of TFE percentage; B. CD spectra of 0.15 mM Ni3 in the 70%: 30% H_2O - TFE solvent mixture as a function of temperature (temperature decreasing from top to bottom at 222 nm). Inset: $-[\theta]_{222}$ as a function of temperature.

to the amphipathic nature of the helix and to the presence of the Tyr Leu pairs, they initially form loose helix associations that can lead to a dampening of the optical activity. As the pH increases, the supramolecular clusters become tighter and, between pH 7.7 and 9.6, an α-helical coiled-coil may form. These molecular events are supported by the changes in the CD spectra consisting of a red shift of the cross-over point and in a drastic reduction of the π-$\pi^*_{\|}$ transition that leads to $[\theta]_{222}/[\theta]_{min} > 1$. The lack of a clear red shift of the π-$\pi^*_{\|}$ transition [36] is probably due to the fact that it is not a simple two-state equilibrium.

In conclusion, in the case of fCT, the driving force responsible for its folding is a combination of various factors such as intramolecular hydrophobic interactions between Leu and Tyr chains [26] as well as the reduction of the repulsive forces between the charged Lys residues [25] and the formation of

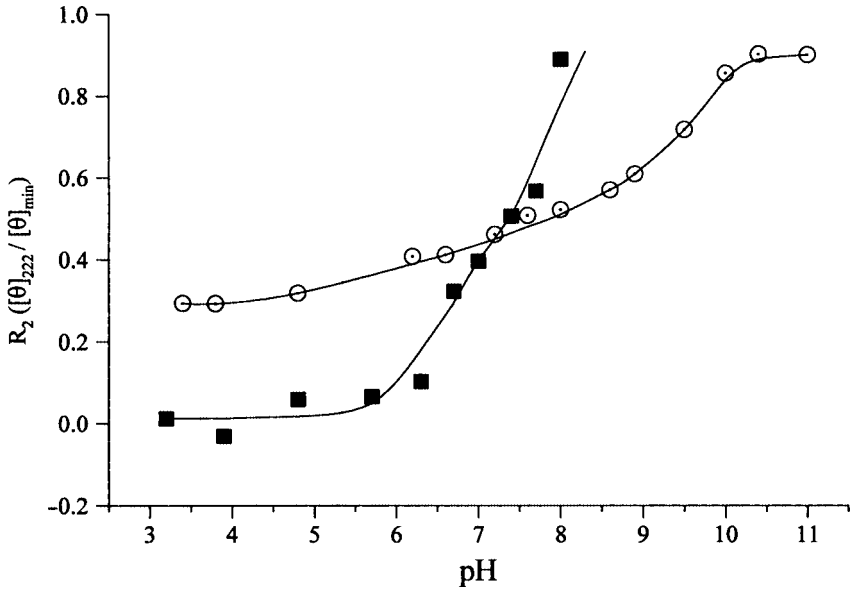

Figure 8 R_2 vs pH for *f*CT (■) and Ni3 (○). R2 is the $[\theta]_{222}/[\theta]_{neg.max}$ ratio, according to [35].

salt bridges between Tyr and Lys residues [27, 28]. These last factors contribute to neutralize the helix surface and to enhance the intermolecular hydrophobic interactions, thus determining the strong aggregation tendency of the peptide that leads to the formation of supramolecular clusters and/or helical coiled-coils [29, 37].

The folding of Ni3, on the other hand, is mostly driven by intramolecular electrostatic interactions. This is evidenced by the shape of the pH titration, where the two conformational transitions centred at pH 6.5 ± 0.1 and 9.4 ± 0.1 (Figure 5A, inset) reflect the dissociation of ionizable residues. In addition, the peptide insensitivity to ionic strength suggests a helical structure with a surface possessing a net high electron density that gives rise to repulsive intermolecular interactions and prevents aggregation.

In TFE, however, where the aggregation processes are strongly hampered, the two peptides behave in a very similar manner. Thus, we can conclude that, although both peptides possess similar helicity, the global folding is driven by diverse chemical interactions that lead to distinct molecular behaviour in aqueous environment.

The Ci3 segment. In water at pH 4.0, Ci3 exists in an extended conformation [15] and, similarly to Ni3, its conformation is insensitive to changes in peptide concentration (data not shown). However, in this case variations of pH and ionic strength do not induce any regular folding of the peptide (data not shown).

The titration with TFE (Figure 9A) shows that, in agreement with NMR data [15], the solvent can favour the formation of some helical determinants, as suggested by the enhancement of the negative band at 220–222 nm. However, the overall folding process occurs in a quite different manner and to a different extent when compared with Ni3 and *f*CT. As a matter of fact, the CD profile does not permit a unique interpretation. In fact, it is possible that the negative band at about 205 nm exists as the result of the coexistence of the α-helix π-$\pi_{\parallel}^{*}$ transition with the random coil π-π^{*} transition, therefore being compatible with a peptide containing α-helix and random coil portions [38]. Such an interpretation is supported by the fact that the first negative band, that in the case of a pure α-helix is at 222 nm, is shifted here to about 220 nm and by the observation that the positive π-$\pi_{\perp}^{*}$ transition at 195 nm is strongly dampened. Alternatively, the two major negative bands in the 202–204 nm and 218–222 nm regions could reflect the presence of structural determinants reminiscent either of a 3_{10}-helix [39] or of turns belonging to a helical backbone and giving rise to a β-spiral-like motif [40, 41].

To further verify the peptide difficulty in acquiring a well-defined secondary structure, we examined the temperature dependence of its structure in 100% TFE. Figure 9B shows that throughout the

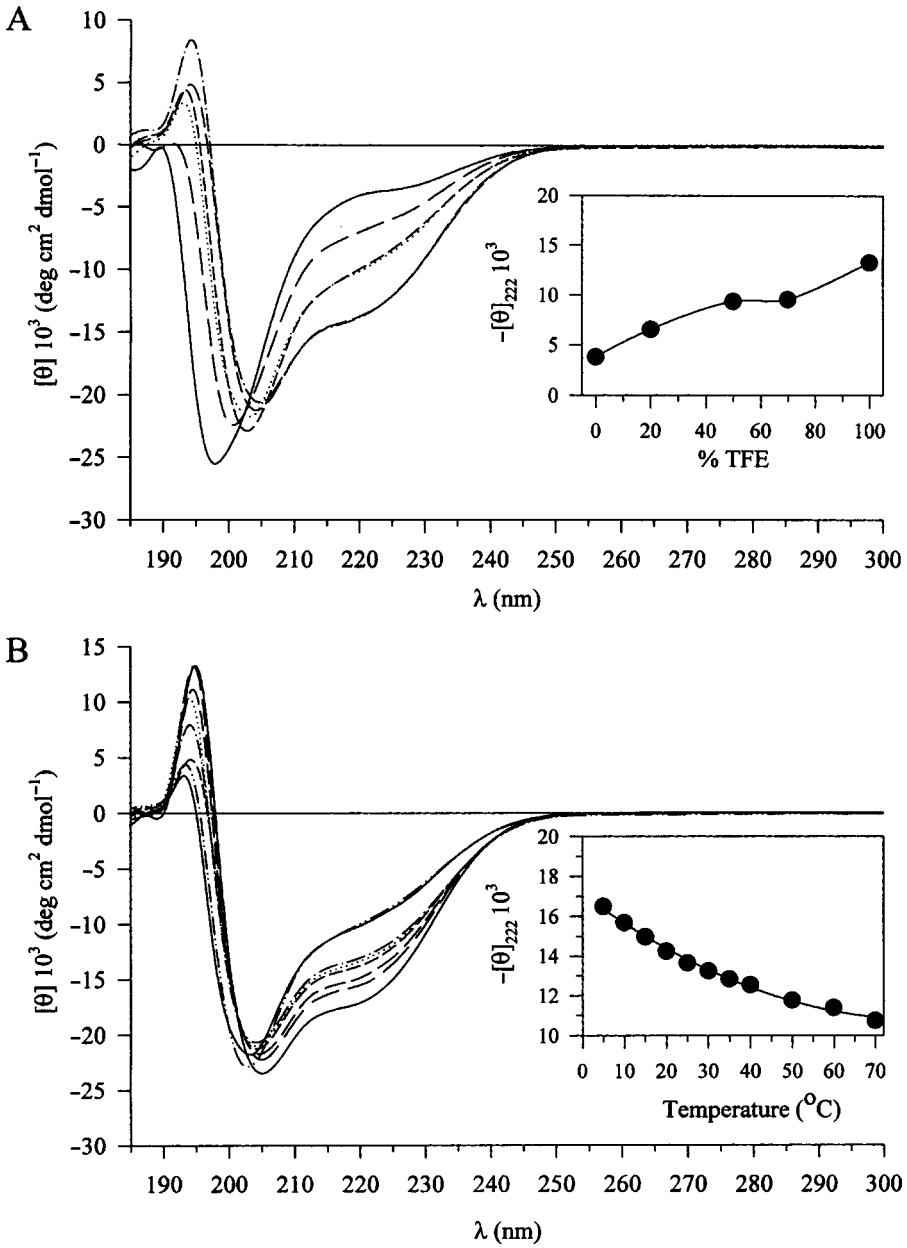

Figure 9 A. CD spectra of 0.15 mM Ci3 in water at pH 4.0 and upon addition of TFE in the concentration range 0–100% (v/v) at 20 °C (TFE concentration increasing from top to bottom at 222 nm). Inset: $-[\theta]_{222}$ as a function of TFE percentage. B. CD spectra of 0.15 mM Ci3 in 100% TFE as a function of temperature (temperature decreasing from top to bottom at 222 nm). Inset: $-[\theta]_{222}$ as a function of temperature.

entire temperature range (5°–70 °C) the CD profile is not indicative of any preferential conformation. In addition, the non-linear variation of the molar ellipticity at 222 nm (Figure 9B, inset) suggests that changes in temperature induce conformational modifications involving the extension and combination of the various secondary structure elements present in the peptide.

CONCLUSION

The present view of the molecular mechanism of signal transduction consists of a sequence of events in which ligand binding induces a concerted reorganization of the spatial distribution of the transmembrane helices [42]. Such a structural change would propagate to the cytosolic loops leading

to a rearrangement of their conformation, the receptor activation. The resulting alteration of the receptor-G protein contacts constitutes the receptor G-protein coupling, responsible for G-protein signalling [42, 43].

Overall conformational flexibility is a key feature for the function of the GPCR machinery. Here we have studied three peptides encompassing functional regions of the AT_{1A} receptor showing that, using *in vitro* conditions that mimic their *in vivo* microenvironment, they can undergo distinct conformational changes that are expected to reflect their specific role in the various steps of AT_{1A} operation.

We believe, therefore, these studies may be useful for better understanding the complex structure–function relationship of large proteins such as GPCRs and, in particular, they may provide insights that will allow the description in a more precise manner of those molecular processes that are often indicated as generic conformational changes.

Acknowledgements

This work was partially supported by grants from FAPESP and CNP_q (A.C.M.P, C.R.N. and S.S.); from MURST and CNR: grants 98.00517.CT04 and 99.02668.CT04 (A.S.). T.A.P. was recipient of a CNP_q doctoral fellowship. S.S., C.R.N and A.C.M.P. are recipients of CNP_q career fellowships. The Centro Interfacoltà Misure of the University of Parma is acknowledged for providing the dicrograph to carry out part of the CD experiments.

REFERENCES

1. Wess J. G-protein-coupled receptors: molecular mechanisms involved in receptor activation and selectivity of G-protein recognition. *FASEB J.* 1997; **11**: 346–354.
2. Wray V, Federau T, Gronwald W, Mayer H, Schomburg D, Tegge W, Wingender E. The structure of human parathyroid hormone from a study of fragments in solution using ^{1}H NMR spectroscopy and its biological implications. *Biochemistry* 1994; **33**: 1684–1693.
3. Pellegrini M, Bisello A, Rosenblatt M, Chorev M, Mierke DF. Binding domain of human parathyroid hormone receptor: from conformation to function. *Biochemistry* 1998; **37**: 12737–12743.
4. Dorey M, Hargrave PA, McDowell JH, Arendt A, Vogt T, Bhawsar N, Albert AD, Yeagle PL. Effects of phosphorylation on the structure of the G-protein receptor rhodopsin. *Biochim. Biophys. Acta* 1999; **1416**: 217–224.
5. Arshava B, Liu SF, Jiang H, Breslav M, Becker JM, Naider F. Structure of segments of a G protein-coupled receptor: CD and NMR analysis of the *Saccharomyces cerevisiae* tridecapeptide pheromone receptor. *Biopolymers* 1998; **46**: 343–357.
6. Gelber EI, Kroeze WK, Willins DL, Gray JA, Sinar CA, Hyde EG, Gurevitch V, Benovich J, Roth BL. Structure and function of the third intracellular loop of the 5-hydroxytryptamine 2A receptor: the third intracellular loop is α-helical and binds purified arrestins. *J. Neurochem.* 1999; **72**: 2206–2214.
7. Shirai H, Takahashi K, Katada T, Inagami T. Mapping of G protein coupling sites of the angiotensin II type 1 receptor. *Hypertension* 1995; **25**(part 2): 726–730.
8. Kai H, Alexander RW, Ushio-Fukai M, Lyons PR, Akers M, Griendling KK. G-Protein binding domains of the angiotensin II AT_{1A} receptors mapped with synthetic peptides selected from the receptor sequence. *Biochem. J.* 1998; **332**: 781–787.
9. Sano T, Ohyama K, Yamano Y, Nakagomi Y, Nakazawa S, Kikyo M, Shirai H, Blank JS, Exton JH, Inagami T. A domain for G protein coupling in carboxyl-terminal tail of rat angiotensin II receptor type 1A. *J. Biol. Chem.* 1997; **272**: 23631–23636.
10. Conchon S, Barrault MB, Miserey S, Corvol P, Clauser E. The C-terminal third intracellular loop of the rat AT_{1A} angiotensin receptor plays a key role in G protein coupling specificity and transduction of the mitogenic signal. *J. Biol. Chem.* 1997; **272**: 25566–25572.
11. Wang C, Jayadev S, Escobedo JA. Identification of a domain in the angiotensin II type 1 receptor determining G_q coupling by the use of receptor chimeras. *J. Biol. Chem.* 1995; **270**: 16677–16682.
12. Shibata T, Suzuki C, Ohnishi J, Murakami K, Miyazaki H. Identification of regions in the human angiotensin II receptor type 1 responsible for G_i and G_q coupling by mutagenesis study. *Biochem. Biophys. Res. Commun.* 1996; **218**: 383–389.
13. Ohyama K, Yamano Y, Chaki S, Kondo T, Inagami T. Domains for G-protein coupling in angiotensin II receptor type I: studies by site-directed mutagenesis. *Biochem. Biophys. Res. Commun.* 1992; **189**: 677–683.
14. Franzoni L, Nicastro G, Pertinhez TA, Tatò M, Nakaie CR, Paiva ACM, Schreier S, Spisni A. Structure of the C-terminal fragment 300–320 of the rat angiotensin II AT_{1A} receptor and its relevance with respect to G-protein coupling. *J. Biol. Chem.* 1997; **272**: 9734–9741.
15. Franzoni L, Nicastro G, Pertinhez TA, Oliveira E, Nakaie CR, Paiva ACM, Schreier S, Spisni A. Structure of two fragments of the third cytoplasmic loop of the rat angiotensin II AT_{1A} receptor. Implications with respect to receptor activation and G-protein selection and coupling. *J. Biol. Chem.* 1999; **274**: 227–235.
16. Atherton E, Sheppard RC. In *Solid Phase Peptide Synthesis: A Practical Approach*. I.L.R. Press: Oxford, 1989.

17. Barany G, Merrifield RB. *The Peptides: Analysis, Synthesis and Biology*, Gross E, Meienhofer J (eds). Academic Press: New York, 1980, **2**: 1–284.
18. Knorr R, Trzeciak A, Bannwarth W, Gillessen D. New coupling reagent in peptide chemistry. *Tetrahedron Lett.* 1989; **30**: 1927–1930.
19. Carpino LA. 1-hydroxy-7-azabenzotriazole. An efficient peptide coupling additive. *J. Am. Chem. Soc.* 1993; **115**: 4397–4398.
20. Cilli EM, Oliveira E, Marchetto R, Nakaie CR. Correlation between solvation of peptide-resins and solvent properties *J. Org. Chem.* 1996; **61**: 8992–9000.
21. Pace CN, Vajdos F, Fu L, Grimsley G, Gray T. How to measure and predict the molar absorption coefficient of a protein. *Protein Sci.* 1995; **4**: 2411–2423.
22. Chen YH, Yang JT, Chau KH. Determination of the helix and β- form of proteins in aqueous solution by circular dichroism. *Biochemistry* 1974; **13**: 3350–3359.
23. Parker CA. *Photoluminescence of Solutions*. Elsevier: Amsterdam, 1968.
24. Eftink MR, Ghiron CA. Fluorescence quenching studies with proteins. *Anal. Biochem.* 1981; **114**: 199–227.
25. Goto Y, Aimoto S. Anion and pH-dependent conformational transition of an amphiphilic polypeptide. *J. Mol. Biol.* 1991; **218**: 387–396.
26. Padmanabhan S, Jiménez MA, Laurents DV, Rico M. Helix-stabilizing nonpolar interactions between tyrosine and leucine in aqueous and TFE solutions: 2D-^{1}H NMR and CD studies in alanine-lysine peptides. *Biochemistry* 1998; **37**: 17318–17330.
27. Hagihara Y, Kataoka M, Aimoto S, Goto Y. Charge repulsion in the conformational stability of melittin. *Biochemistry* 1992; **31**: 11908–11914.
28. Scholtz JM, Baldwin RL. The mechanism of α-helix formation by peptides. *Annu. Rev. Biophys. Biomol. Struct.* 1992; **21**: 95–118.
29. Zhou NE, Kay CM, Hodges RS. Synthetic model proteins. Positional effects of interchain hydrophobic interactions on stability of two-stranded α-helical coiled-coils. *J. Biol. Chem.* 1992; **267**: 2664–2670.
30. Marqusee S, Baldwin RL. Helix stabilization by Glu– . . . Lys+ salt bridges in short peptides of *de novo* design. *Proc. Natl. Acad. Sci. USA* 1987; **84**: 8898–8902.
31. Lakowicz JR. *Principle of Fluorescence Spectroscopy*. Plenum Press: New York, 1983.
32. Ross JBA. *Biochemical Fluorescence Concepts*, Chen RF, Edelhoch H (eds). Dekker: New York, 1977.
33. Sönnichsen FD, Van Eyk JE, Hodges RS, Sykes BD. Effect of trifluoroethanol on protein secondary structure: an NMR and CD study using a synthetic actin peptide. *Biochemistry* 1992; **31**: 8790–8798.
34. Rajan R, Balaram P. A model for the interaction of trifluoroethanol with peptides and proteins. *Int. J. Pept. Protein Res.* 1996; **48**: 328–336.
35. Bruch MD, Dhingra MM, Gierasch LM. Side chain-backbone hydrogen bonding contributes to helix stability in peptides derived from an α-helical region of carboxypeptidase A. *Protein Struct. Funct. Genet.* 1991; **10**: 130–139.
36. Cooper TM, Woody RW. The effect of conformation on the CD of interacting helices: a theoretical study of tropomyosin. *Biopolymers* 1990; **30**: 657–676.
37. Collawn JF, Paterson Y. Stabilization of helical structure in two 17-residue amphipathic analogues of the C-terminal peptide of cytochrome C. *Biopolymers* 1990; **29**: 1289–1296.
38. Shoemaker KR, Kim PS, York EJ, Stewart JH, Baldwin RL. Tests of the helix dipole model for stabilization of α-helices. *Nature* 1987; **326**: 563–567.
39. Toniolo C, Polese A, Formaggio F, Crisma M, Kamphuis J. Circular dichroism spectrum of a peptide 3_{10}-helix. *J. Am. Chem. Soc.* 1996; **118**: 2744–2745.
40. Urry DW. Characterization of soluble peptides of elastin by physical techniques. *Methods Enzymol.* 1982; **82**: 673–716.
41. Urry DW, Venkatachalam CM, Long MM, Prasad KU. In *Conformation in Biology*, Srinivasan R, Sarma RM (eds). Academic Press: New York, 1983; 11–27.
42. Inoue Y, Nakamura N, Inagami T. A review of mutagenesis studies of angiotensin II type 1 receptor, the three-dimensional receptor model in search of the agonist and antagonist binding sites and the hypothesis of a receptor activation mechanism. *J. Hyperten.* 1997; **15**: 703–714.
43. Bourne HR. How receptors talk to trimeric G proteins. *Curr. Opin. Cell. Biol.* 1997; **9**: 134–142.

